II. MATERIALS AND TECHNIQUES

toroidal particles and defects around them were realized with a holographic optical trapping (HOT) system [27,34] operating at a wavelength of $\lambda = 1064$ nm and using the same objectives as for the conventional optical and nonlinear 3PEF-PM imaging.

III. RESULTS

FIG. 2. Edge-pinned defect lines around a particle in a twisted nematic cell: (a,b,d,e) Optical micrographs obtained between crossed (a,d,e) and parallel (b) polarizers P and A. Orientation of a pair of bulk $\check{S} 1/2$ defects (shown by black arrows) inside a particle's ring in (a) and (d) is different with respect to $\mathbf{P}$. Inset in (b) shows right-handed twist of $\mathbf{n}(\mathbf{r})$ between bottom and top substrates with orthogonal easy axes $\mathbf{e}_b$ and $\mathbf{e}_t$, respectively. (e) Optical texture showing a zoomed-in view of a bulk $\check{S} 1/2$ defect line seen in (d)
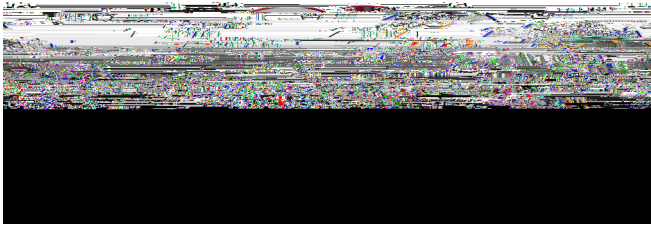
FIG. 3. Detailed schematic diagrams n(r) and defects in the
region of transformation of disclinations inside (a) and outside (c) of
a toroidal particle with square-shaped cross section (b). The handle-
shaped bulk defect lines are depicted as thick red lines. The quarter-
strength edge-bound surface defect lines of opposite signs are shown
using thin blue and orange lines, with the strength of opposite signs
marked next to them. The green lines depict the director field.

index within the studied medium such as our LC-colloidal
composite, yet they are powerful tools to study them. The
important feature to notice here is that, upon tilting the torus,
the far ends of both outer and inner bulk disclinations with
respect to a tilt axis absorb to opposite – top and bottom – edges
of the colloidal torus [Figs. 1(g), 1(l), 1(m), and 3]. These
newly formed structures with negative quarter defects, both
at the inner and outer sides, propagate along opposite circular
edges towards the middle of the torus to a branching point/node
where they desorb from the edge and continue as the positive
quarter defect and the bulk half-integer defect line jumping
from the top to bottom edges (Fig. 3), as can be deduced
from the experimental observations [Figs. 6(b) and 2(e)].
Interestingly, each of the four circular edges has two quarter
disclination arcs of an opposite sign meeting at the branching
points connected by bulk half-integer disclination fragments
(Fig. 3). The typical length of these bulk fragments is about the
side width $\approx 5 \, \mu$m of a square-shaped tube forming the ring
[Fig. 2(e)]. Topological transformation at the branching node
conserves the strength of defect lines: the

with respect to each other, naturally defining the ubiquitous appearance of quarter-strength surface-bound nematic defect lines, the control of geometric shape (e.g., the control of angles of misalignment between faces at sharp edges of concave and convex particles of different geometry [26,31,43]) may allow for variable strength k of the particle-induced surface defect lines. In future works, therefore, it will be even more interesting to explore how the surface-bound defect lines with unconstrained k, such as, for example, $k = +1/6$ or $k = −2/9$ surface defect lines, can then transform into the bulk defect lines constrained to have $|k| = 1/2$ and vice versa. It will also be of interest to explore how the strength of surface anchoring, in addition to faceted-shape geometry, can determine k values and the behavior of these defects. For example, the finite surface anchoring strength can cause departures of k values of disclinations pinned to the $90°$ edges between flat particle faces away from $k = ±1/4$. In general, the richness of possibilities that can arise can be modeled by placing normal nematic disclinations with $k = ±1/2$ and considering the k values as defined within the LC bulk that remains after the virtual part of this defect line is depressed inside the colloidal particle with a

FIG. 6. Deformation of bulk disclinations around torus-shaped colloidal particles in a nematic LC. (a) Bright-field optical micrograph of a tilted particle with an outer bulk half-integer disclination that is not absorbed at the particle edges. Inset shows a corresponding polarizing microscopy texture obtained between crossed polarizers P and A. Black and white (in the inset) thin arrows mark points where the deformed outer half-integer defect loop transitions between the top and bottom edges. (b) A schematic diagram showing the corresponding $\mathbf{n}(\mathbf{r})$.

we show that many types of defect structures can nonetheless occur to match the strong boundary conditions on faceted rings to that of the uniform far-field director. The large variety of observed colloidal-defect structures additionally demonstrates that colloidal handle-body-shaped particles [26,30] suspended in an anisotropic LC host fluid can access a wide variety of metastable states and cause unusual transformations of defects not accessible to defects induced by spherical inclusions, or even geometrically complex colloidal inclusions with the simple genus-zero topology. Further, our study in this work demonstrates that the size of ring-shaped particles matters and that the particles with large cross-section dimensions relative to the surface anchoring extrapolation length can exhibit behavior different from that of small colloids with the same topology and geometric features [28].

IV. DISCUSSION

All previous studies of LC-colloidal systems dealt with either surface or bulk particle-induced defects, but our experiments described above demonstrate that the bulk and surface defects can coexist in the LC surrounding of the same particle and can even transform from one type to another, forming nodes of bulk and surface defect lines. These observations highly enrich the interplay between the topologies of colloidal surfaces and nematic field configurations that they induce in the uniform LC background. Although we studied ring-shaped particles with edges connecting flat and curved faces at $90°$

the edges around a particle [Figs. 1(j) and 1(k)] or an elastic
quadrupole with symmetry of a nematic